Article

Soil Water Extraction Monitored Per Plot Across a Field Experiment Using Repeated Electromagnetic Induction Surveys

Jingyi Huang [1],*, Ramamoorthy Purushothaman [2], Alex McBratney [1] and Helen Bramley [2] 🆔

[1] Sydney Institute of Agriculture & School of Life and Environmental Sciences, The University of Sydney, Eveleigh, NSW 2015, Australia; alex.mcbratney@sydney.edu.au

[2] Plant Breeding Institute, Sydney Institute of Agriculture & School of Life and Environmental Sciences, The University of Sydney, 12656 Newell Highway, Narrabri, NSW 2390, Australia; purushothaman.ramamoorthy@sydney.edu.au (R.P.); helen.bramley@sydney.edu.au (H.B.)

* Correspondence: xuehaiwuya8@gmail.com

Abstract: Soil water (θ) dynamics are important parameters to monitor in any field-based drought research. Although apparent electrical conductivity (EC_a) measured by electromagnetic (EM) induction has been used to estimate θ, little research has shown its successful application at the plot-scale for evaluating crop water use. An EM38 conductivity meter was used to collect time-lapse EC_a data at the plot scale across a field cropped with 36 different chickpea genotypes. An empirical multiple linear regression model was established to predict θ measured by neutron probes and depth-specific electrical conductivity (σ) generated by a 1-D EM inversion algorithm. Soil water dynamics and movement were successfully mapped with a coefficient of determination (R^2) of 0.87 and root-mean-square-error of 0.037 m^3 m^{-3}. The rate of soil drying varied with depth and was influenced by chickpea growth stages and genotypes. The results were also used to evaluate the differences in soil water use and rooting depths within- and across-plant species and during the growth stages. Coupled with physiology measurements, the approach can also be used to identify mechanisms of drought tolerance in the field and screening for effective water use in crop breeding programs.

Keywords: EM38; EM inversion; chickpea; genotypes; drought-tolerance; water use

1. Introduction

Monitoring soil water content at different depths and its dynamics can be used to determine plant water use and hence, water use efficiency. The ability to do this at the plot level on a meaningful scale has been considered impractical by plant breeders [1], so that selection for drought-tolerant and more effective water use in the field has been limited [2]. Measuring soil volumetric water content (θ) in the laboratory using the thermogravimetric method is labour-intensive [3]. Indirect methods to estimate θ in the field have been used, such as neutron probes, time domain reflectometry, capacitance probes, and electrical resistivity tomography [4,5], but these instruments need to be installed into the soil profiles, which is time-consuming and expensive, and hinders their potential applications for estimating θ at depths, across larger spatial extents and hundreds of plots. In addition, some agricultural practices (e.g., ploughing) may not be possible if sensors are permanently installed in the soil (especially at shallow depth).

Recently, non-invasive electromagnetic induction (EMI) instruments have been successfully used in the field to estimate and map θ within the root-zone and vadose zone [6,7]. Estimation of θ with EMI is possible because the measured soil apparent electrical conductivity (EC_a) is directly

and indirectly correlated with clay content, salinity, θ, cation exchangeable capacity, available water content and crop yield [8–11]. By conducting time-lapse EMI surveys, it may be possible to retrieve θ dynamics by establishing empirical models either using EC_a data [12–14] or estimates of depth-specific electrical conductivity (σ) generated by EM inversion algorithms [15,16]. These models have been successfully used to map θ dynamics across a field associated with homogenous sandy soils [16,17] and texture-varying soils comprising loams and medium clays [18]. However, estimation of soil water content using EMI data only is not always straightforward and not always possible (see [19–23]). In addition, apart from a few studies (e.g., [20]), the feasibility of using EMI for monitoring θ dynamics and studying crop water use at the plot scale has not yet been documented.

Therefore, the aims of this study were to: (1) establish an empirical model to estimate θ dynamics using time-lapse EC_a datasets collected by a Geonics EM38 conductivity meter across 40 chickpea plots (each plot 1.6 × 4 m) with different water treatments (i.e., rainfed and irrigated), (2) predict θ dynamics at various soil depths at the plot scale across 288 plots after a rainfall event, and (3) compare different evapotranspiration rates associated with treatments and genotypes and provide guidance for screening drought tolerant genotypes.

2. Materials and Methods

2.1. Study Site

The study field was located on an experimental farm of the Plant Breeding Institute of The University of Sydney (Figure 1), Narrabri, NSW, Australia (30°16′31.7″ S, 149°48′10.7″ E). The location has a sub-tropical climate with mean annual maximum and minimum temperature of 26.5 and 11.7 °C, respectively, and mean annual precipitation of 663 mm [24]. The site of the trial consisted of a deep black cracking clay soil, characterised as a Vertosol [25], which had been cropped with barley in the previous winter season and had not been tilled. Around 10 cm of standing stubble remained. Weeds were controlled with commercial herbicides before sowing and hand-pulling during the experiment.

The trial area was 0.6 ha (180 m × 32 m) orientated in a northeast-southwest direction and divided equally into two blocks (Figure 1). The northeast block was rainfed only, while the southwest half received 25 mm irrigation (total 100 mm) approximately every two weeks from mid-August, which was applied homogeneously to the field using a lateral move irrigator. Each treatment block contained 144 plots and each block was surrounded by two rows of the buffer. Each plot was 1.6 m × 6 m, which was cut back to 4 m on 1 September 2017. The trial design was an incomplete block design with four replicate plots per genotype per treatment (rainfed and irrigated).

Thirty-six different chickpea (*Cicer arietinum*) genotypes, consisting of breeding lines and commercial cultivars, were sown on 5 June 2017, which is within the planting window recommended for northern New South Wales. The buffer plots were sown with the cultivar PBA Seamer. Seeds were pre-treated with fungicides and sown at a rate of 30 plants m^{-2} using a five-row mechanical planter with inter-row spacing 0.32 m. Granulated inoculant (Nodulator®, Group-N Granular Legume Inoculant, BASF Australia Limited, Southbank Victoria, Australia) at a rate of 3.2 kg ha^{-1} and Granulock Z Extra fertiliser (Granulock®, Incitec Pivot Limited, Port Lincoln, SA, Australia) at a rate of 50 kg ha^{-1} were also applied at the time of sowing. The initial and final EM38 measurements were taken on 19 October 2017 and 3 November 2017, respectively. At this stage, the genotypes under rainfed condition were close to physiological maturity whereas the genotypes under irrigated condition were at the late pod-filling stage.
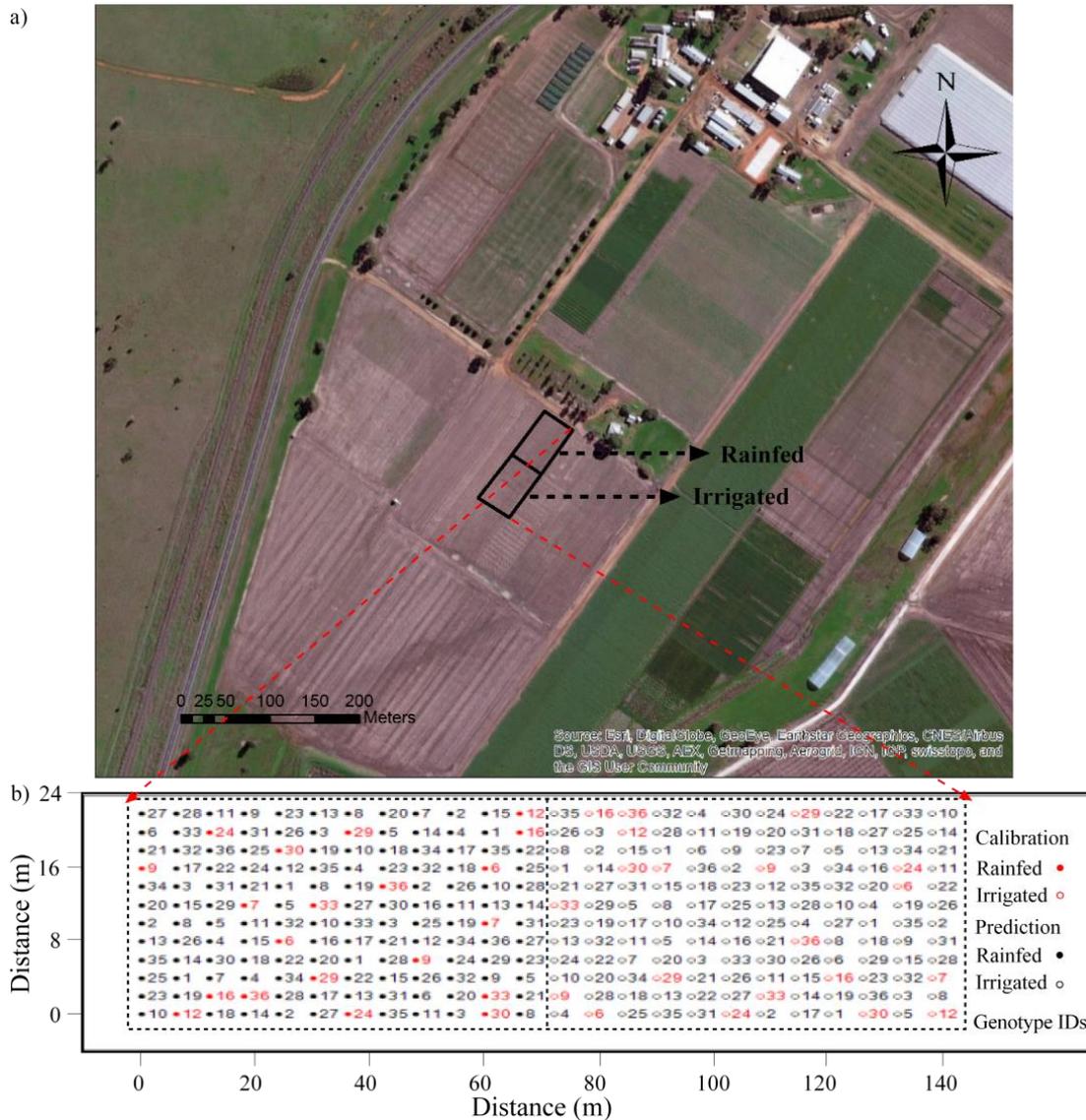
Figure 1. (**a**) Location of the experimental field in the Plant Breeding Institute, The University of Sydney, Narrabri, New South Wales, Australia; (**b**) Locations of the chickpea genotypes and the rainfed (closed circles) and irrigated (open circles) treatments. Note: the red circles indicate plots where access tubes were installed, which were used for calibrating the empirical model for predicting soil water dynamics; the dash lines in Figure 1b indicated boundaries of the irrigated and rainfed plots.

2.2. Geonics EM38 Configuration

An EM38 (Geonics Ltd., Mississauga, ON, Canada) conductivity meter provides EC_a measurements in the root zone. The depths of exploration (DOE) of the EM38 are 1.5 m in the vertical (EM38v) and 0.75 m in the horizontal (EM38h) modes of coil orientation when the instrument is placed on the ground surface [26]. When the height of the instrument is raised, EC_a decreases. EC_a data collected at multiple heights can be used to improve modelling of the shallow earth structure [26]. This was the approach of various previous studies [27–29] and it was adopted in this study.

2.3. Time-Lapse EM38 Surveys

To establish an empirical calibration model to predict θ dynamics, EC_a data were collected across 20 plots in the irrigated section on 1 day before (1 October 2017) as well as 2 (5 October 2017),

3 (6 October 2017), 4 (7 October 2017), and 5 (8 October 2017) days after a 25-mm irrigation event (Figure 1). EC_a data were also collected across 20 rainfed plots on the same days (Figure 1). EC_a data were measured in both EM38v and EM38h modes and at five different heights (i.e., 0 m, 0.2 m, 0.4 m, 0.6 m and 0.8 m). EC_a data were collected close to the centre of each plot where an aluminium access tube was installed.

To compare the water use of chickpea associated with different treatments and genotypes, repeated EM38 surveys were also measured on all 288 plots at the same heights and 1 (23 October 2017), 3 (25 October 2017), 9 (31 October 2017) and 12 (3 November 2017) days after a rainfall event (~12.6 mm of water).

Temperature has previously been reported to influence the temporal and spatial pattern of data suggesting the need for temperature correction [12,22,30–35]. Based on our previous experiment [36], we inferred that the change of soil temperature in a Vertosol with large specific heat capacity and covered with an enclosed crop canopy would be less than 2 °C at 0–0.2 m during our experiment and the change would decrease with increasing depth. This would lead to a shift of EC_a of approximately 3.8% in the field due to diurnal soil temperature fluctuation at 0–0.2 m and a shift of less than 3.8% below 0.2 m. Based on the minor impact of this estimation, we chose not to correct the EC_a based on soil temperature.

Because diurnal drifts of EMI instruments due to ambient temperature have also been reported [36,37], preliminary EC_a measurements were taken before the irrigation event at three selected locations at different times of the day when the temperature ranged between 20 and 35 °C. Diurnal drifts were found to be negligible (<1 mS m^{-1}) once the EM38 meter was calibrated according to the user manual prior to the survey. All the EM38 surveys in this study were completed within this temperature range and therefore, the measured EC_a data were assumed to be stable.

2.4. Collection of Neutron Probe Measurements

To calibrate the EM38 EC_a data, neutron probe readings were also measured in the 20 rainfed plots and the 20 irrigated plots on the respective days when the EM38 surveys were carried out. The neutron probe readings (CPN® 503DR Hydroprobe, CPN International, Concord, CA, USA) were collected in the access tube at 0.1, 0.2. 0.3, 0.4, 0.5, 0.6, 0.8, 1.0 1.2 and 1.4 m depths. A pre-defined universal calibration formula was employed to convert the neutron counts to soil volumetric water content (θ):

$$\theta = (\text{Neutron counts} - 7863)/182.9 \tag{1}$$

2.5. Inversions of EM38 Data

Because the 40 calibration plots were randomly located across the whole field (Figure 1), a 1-D inversion algorithm was employed. The inversion algorithms [38] were embedded in the EM4Soil Version 3.02 (EMTOMO 2017, http://www.emtomo.com/). In brief, the algorithm aimed at generating estimates of depth-specific electrical conductivity using the cumulative function of EM field in the soil [26]. This study applied an initial model which included 11 layers with the middle depths of the first 10 layers equaling to 0.1, 0.2, 0.3, 0.4, 0.5, 0.6, 0.8, 1.0, 1.2, 1.5 m and the 11th layer at infinity.

2.6. Predicting θ Using an Empirical Model

An empirical calibration model was required to convert σ to θ. Given the dependence of θ on σ and the soil depth (Figure 2a,b), a multiple linear regression (MLR) model was fitted to predict θ using σ and the soil depth. The model parameters were fitted using ordinary least squares with JMP 10.2 (SAS Institute Inc., Cary, NC, USA). Once the model was fitted, it was applied to the whole field to predict θ at different depths across the 288 plots over the 11-day period after the rainfall event.
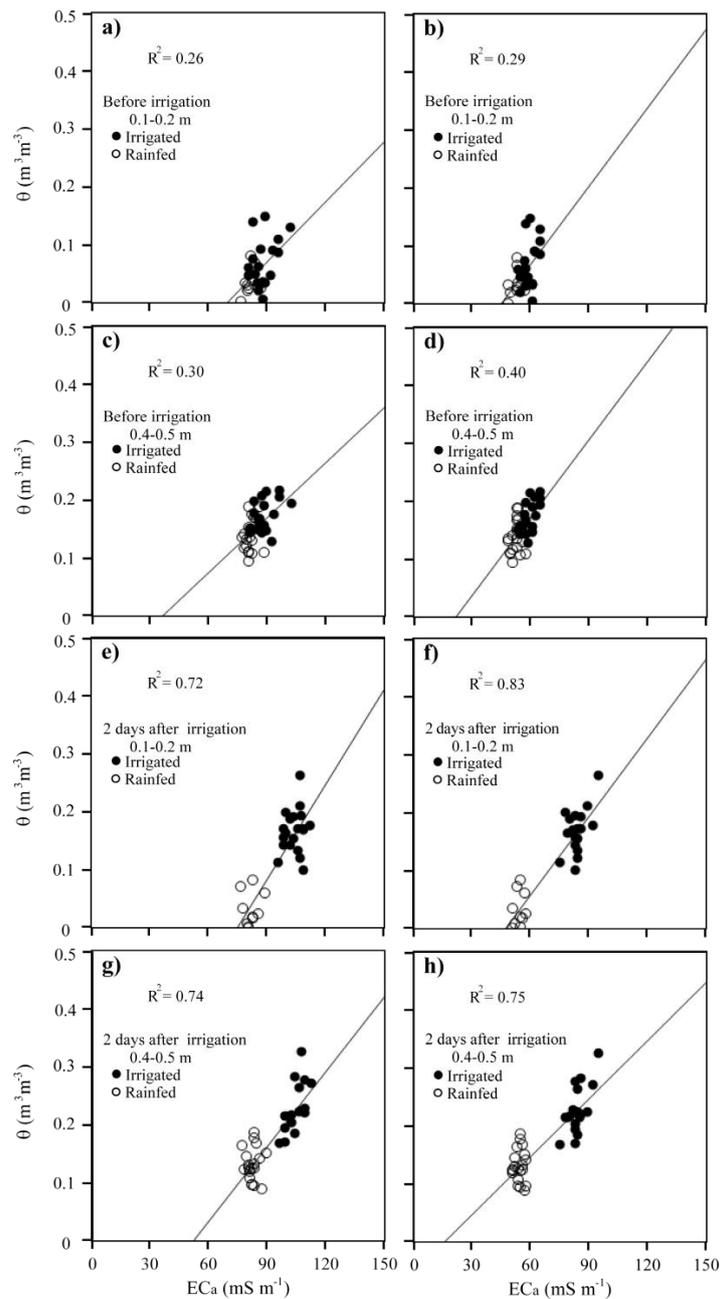
Figure 2. The relationship between measured soil volumetric water content (θ, m^3 m^{-3}) at different depths and measured apparent electrical conductivity (EC_a, mS m^{-1}) by an EM38 on the ground surface with different modes (horizontal—EM38h and vertical EM38v) before irrigation including (**a**) θ at 0.1–0.2 m versus EM38h; (**b**) θ at 0.1–0.2 m versus EM38v; (**c**) θ at 0.4–0.5 m versus EM38h; and (**d**) θ at 0.4–0.5 m versus EM38v and 2 days after irrigation including (**e**) θ at 0.1–0.2 m versus EM38h; (**f**) θ at 0.1–0.2 m versus EM38v; (**g**) θ at 0.4–0.5 m versus EM38h; and (**h**) θ at 0.4–0.5 m versus EM38v.

2.7. Estimating θ Dynamics in 3-Dimensions

To better visualise and interpret θ dynamics in 3-D across the field, the change in predicted θ ($\Delta\theta$) generated by MLR at various depths across the field was calculated based on the first day after irrigation. The water flux (J_{Depth}, mm) within different depth intervals down to 1.2 m (negligible changes of θ below 1.2 m) and between 0 and 1.2 m across the rainfed and irrigated fields were also calculated.

2.8. Comparing Water Use of Different Genotypes

To compare the water use of various chickpea genotypes, we fitted a linear mixed effect model as follows:

$$\Delta\theta = \alpha X + \beta Y + \gamma \text{Genotype} + \delta \text{Treatment} + \zeta \text{Genotype} \times \text{Treatment} + \eta + \varepsilon \qquad (2)$$

Herein, $\Delta\theta$ was the change of θ within 0–1.2 m across the 288 plots during the first 11 days after the irrigation event. The fixed effects included the following variables: X and Y were the distance between the plots as shown in Figure 1; Genotype contained 36 values and were labelled from 1 to 36 due to confidentiality issue; Treatment had two values (i.e., rainfed and irrigated); Genotype × Treatment referred to the interaction between genotype and treatment. η referred to the spatial random effect and was modelled with a semi-variogram; ε was the error. In this study, the parameters of the linear mixed model were fitted using the restricted maximum likelihood (REML) [39]. The geoR package [40] in R was used to fit the model parameters.

In this study, the mean water flux (J_{Depth}, mm) within different depth intervals was also calculated for several selected genotypes (with largest and smallest fixed effects). These values would be used to infer the rooting depths and root activities during the experiment. Herein, we did not fit a linear mixed effect model for every genotype because we did not have a sufficient number of sites to estimate a variogram.

3. Results and Discussion

3.1. Correlation Between θ and EC_a

Figure 2 shows the plot of measured θ at two depths versus EC_a on different days. Figure 2a,b show the plots of measured θ at 0.1–0.2 m versus EC_a measured by EM38h and EM38v, respectively, before irrigation (close to permanent wilting point). In general, EC_a increased with increasing θ but the correlations were weak (R^2 = 0.26 and 0.29). Not surprisingly, similar patterns were observed between irrigated and rainfed plots because the soils in both plots were dry. Figure 2c,d show the plots of measured θ at 0.4–0.5 m versus EC_a measured by EM38h and EM38v, respectively, before irrigation. Similar but slightly stronger correlations were found between θ with EC_a measured by EM38h and EM38v (R^2 = 0.30 and 0.40).

Figure 2e–f show the plots of measured θ at two depths versus EC_a measured by EM38h and EM38v and 2 days after irrigation (close to field capacity). In this case, the correlations between θ with EC_a measured by EM38h and EM38v were much stronger (R^2 = 0.72, 0.83, 0.74 and 0.75) than those identified when the soil was dry. The increase in correlation was mainly because there was a broader range in measured θ as well as EC_a values when the soil became wetter.

It was also worth noting that the correlations between θ and EC_a were different for different depths and different times (soil moisture conditions). Some researchers [23] reported a similar relationship between θ and measured EM38 EC_a in Vertosols, and they also found that the relationship varied with soil depth. The difference in this study was because ECa represented the depth-average soil electrical conductivity with different measurement modes (EM38h and EM38v) corresponding to different DOEs. Therefore, different regression models were required to predict q at different depths using the same set of EC_a data. Based on the results, it is necessary to apply the inversion algorithms to convert EC_a to depth-specific σ and use it for modelling θ.

3.2. Correlation Between θ with σ and Soil Depth

Figure 3a shows the plot of measured θ versus estimated σ across 40 calibration plots over 4 days. In general, σ increased with increasing θ. More importantly, it was worth noting that the overall correlation between θ and σ was stronger than those calculated between θ and EC_a at different depths and on different days (Figure 2). This was not unexpected because the depth-specific σ has a similar

measuring volume compared to θ while EC_a represented the depth-average soil electrical conductivity. Some researchers [16] identified a curve-linear relationship between θ and σ in homogenous loamy soils, which supports these findings. Herein, the soil was similarly uniform but had a medium to high clay content (i.e., Vertosols).

Figure 3b shows the plot of measured θ versus the soil depth. In general, θ increased with the soil depth, which is to be expected because Vertosols normally have a high field capacity (>0.5 m^3 m^{-3}) and permanent wilting point (>0.4 m^3 m^{-3}). Vertosols can hold a large amount of water at depths even when the shallow soils become drier due to evaporation and transpiration.
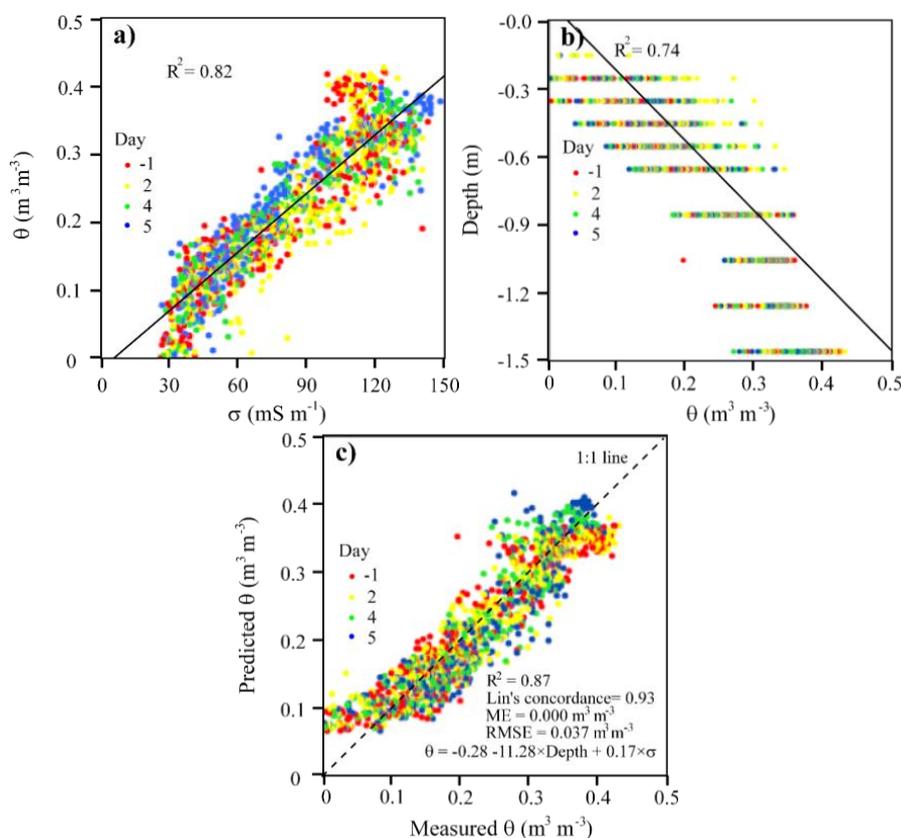
Figure 3. The relationship between measured soil volumetric water content (θ, m^3 m^{-3}) and (**a**) estimated depth-specific electrical conductivity (σ, mS m^{-1}); (**b**) soil depths; and (**c**) predicted θ using 10-fold leave-one-out cross-validation with a multiple linear regression model.

3.3. The Empirical Model of θ

Given the strong correlation between θ with σ and soil depth, a multiple linear regression (MLR) model was established. The model parameters are shown in Figure 3c. Figure 3c also shows 10-fold cross-validation results of the established MLR model. In general, the model performance was good given that Lin's concordance [41] was 0.93, root-mean-square-error (RMSE) was 0.037 m^3 m^{-3} and mean-error (ME) was 0.000 m^3 m^{-3}, respectively. Given the good performance of the MLR model, a non-linear regression model was not fitted and compared in this study.

Figure 3c also shows that the MLR model tended to over-estimate θ values < 0.1 m^3 m^{-3}, which were mostly found in the topsoil. This divergence between measured and predicted θ is most likely caused by the poor performance of the Neutron probe calibration formula for topsoil due to the radiation escaping from the soil surface [42]. In addition, this over-estimation of θ could be due to the uncorrected shift of EC_a due to soil temperature, particularly within 0–0.2 m.

It should be noted that apart from θ, a number of soil properties also influence EC_a, including clay content, soil salinity, the electrical conductivity of the soil solution, and soil temperature [6,22,31,43]. In this study, the coefficient of variation (CV) of EM38v and EM38h measured at the ground surface across the 288 plots was small prior to rainfall (5% and 8%, respectively) and it is expected that the CV values will be smaller if there was no crop in the field. These suggest that the soils are relatively homogenous across the field and these factors are not likely to influence the accuracy of the MLR model established in this study. However, it should be noted that MLR model is site-specific and may not be readily applicable to other areas because of the variation of soil properties in space and time [35,44,45].

3.4. Spatial Distribution of Model Residuals Across the Field

Figure 4 shows the contour plots of the spatial distribution of the MLR model residuals (measured θ–predicted θ) at two depth intervals (0.1–0.2 m and 0.4–0.5 m) across the field before and 2 days after irrigation. In general, the residuals were negative (over-estimation) in the rainfed plot and positive (under-estimation) in the irrigated plot. This was most likely because θ in the rainfed plot was larger than that in the irrigated plot due to the low evapotranspiration rate of the mature chickpeas in the rainfed plot (refer to Figures 1 and 2). Furthermore, it was noted that the residuals in the irrigated plot were more negative at 0–0.1 m than at 0.4–0.5 m, which can be due to either the inaccurate estimation of θ from neutron probe measurements close to the ground surface or the uncorrected drift of EC_a due to soil temperature fluctuations within 0–0.2 m.
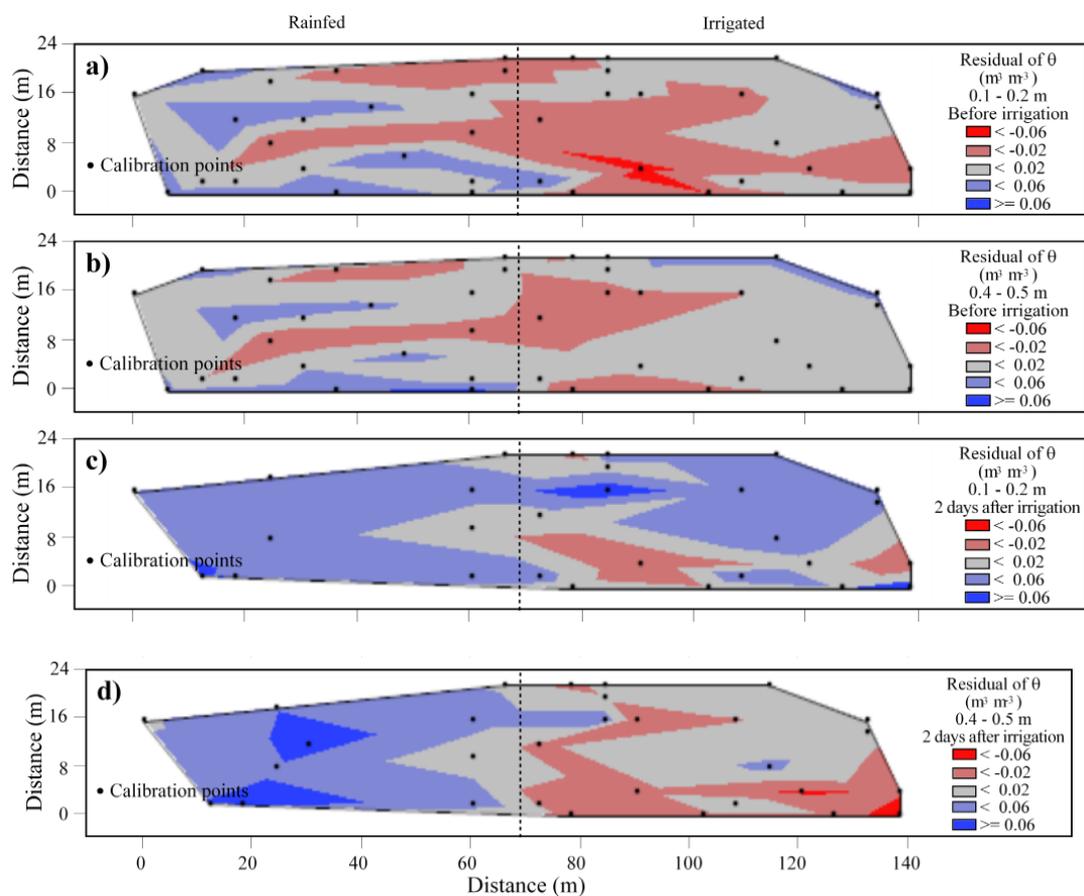
Figure 4. Contour plots of the spatial distribution of the MLR model residuals (measured θ–predicted θ) across the field at (**a**) 0.1–0.2 m and (**b**) 0.4–0.5 m before and (**c**) 0.1–0.2 m and (**d**) 0.4–0.5 m 2 days after irrigation.

3.5. Predicted θ Dynamics Across the Field

Because the day-to-day change in θ was small, the change in θ (Δθ) of a specific day was plotted compared with the first day after the rainfall event. Figure 5 shows the Δθ at various depths across the 288 plots during day 1 and day 3 (2-day period) after the rain.
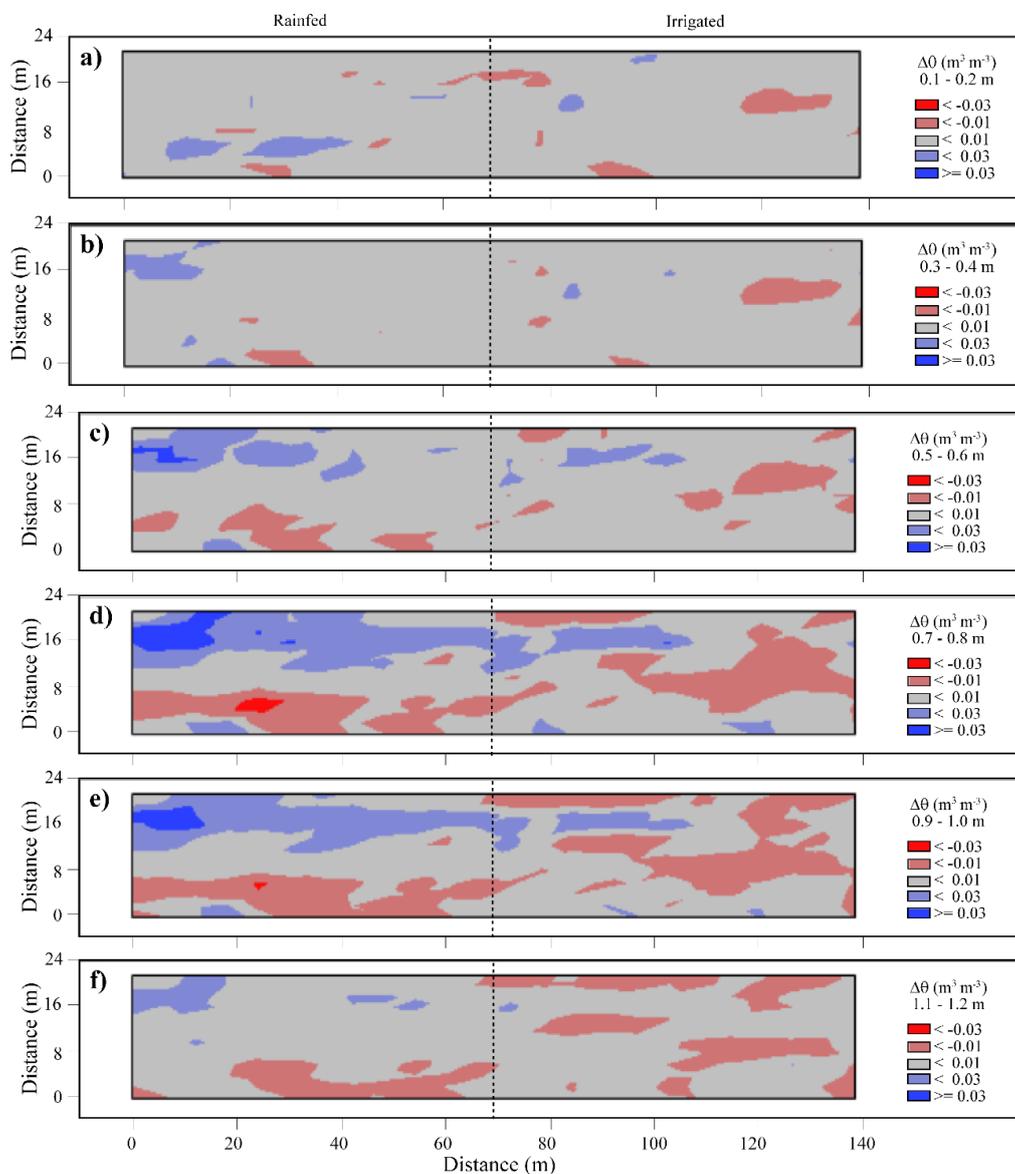
Figure 5. Contour maps of predicted change in soil volumetric water content (Δθ, m³ m⁻³) between 1 and 3 days after a rainfall event (2-day period) at depth intervals (**a**) 0.1–0.2 m; (**b**) 0.3–0.4 m; (**c**) 0.5–0.6 m; (**d**) 0.7–0.8 m; (**e**) 0.9–1.0 m; (**f**) 1.1–1.2 m.

In general, θ was constant at the depth interval of 0.1–0.2 m for most parts of the field (Δθ: -0.01−-0.01 m³ m⁻³) except a few plots in the rainfed side of the field that became slightly wetter (Δθ: 0.01−-0.03 m³ m⁻³) while a few plots in the irrigated half became slightly drier (Δθ: -0.03−-0.01 m³ m⁻³) (Figure 3a). This is consistent with the chickpea genotypes in the rainfed section extracting less water from the soil as they approached physiological maturity compared with the immature chickpea in the irrigated plots, which were still actively taking up water.

Similar patterns in Δθ were observed at other depths but with a few notable differences (Figure 5b–f). In the northern and central rainfed plots, soils at 0.5–1.0 m depths became wetter.

This indicated that water infiltrated down the profiles, probably as preferential flows via the cracks in the Vertosols. In the irrigated plots and the southern end of the rainfed plots, soils were drying faster with increasing depth. This suggested that the chickpea root system was more active at these deeper depths when extracting water from the soils.

Figure 6 shows Δθ across the 288 plots during day 1 and day 9 (8-day period) after the rain. In the rainfed plots, soils dried out at 0.1–0.2 m depth, remained unchanged at the depth of 0.3–0.4 m and became wetter below 0.5 m. This indicated that the evapotranspiration rate of chickpea in the rainfed plots was very low so that the surface drying was mostly caused by evaporation and the subsoil wetting was due to the infiltration of water with time. In the irrigated plots, soils were drying out throughout the whole profile indicating water uptake by chickpea roots across the profile.
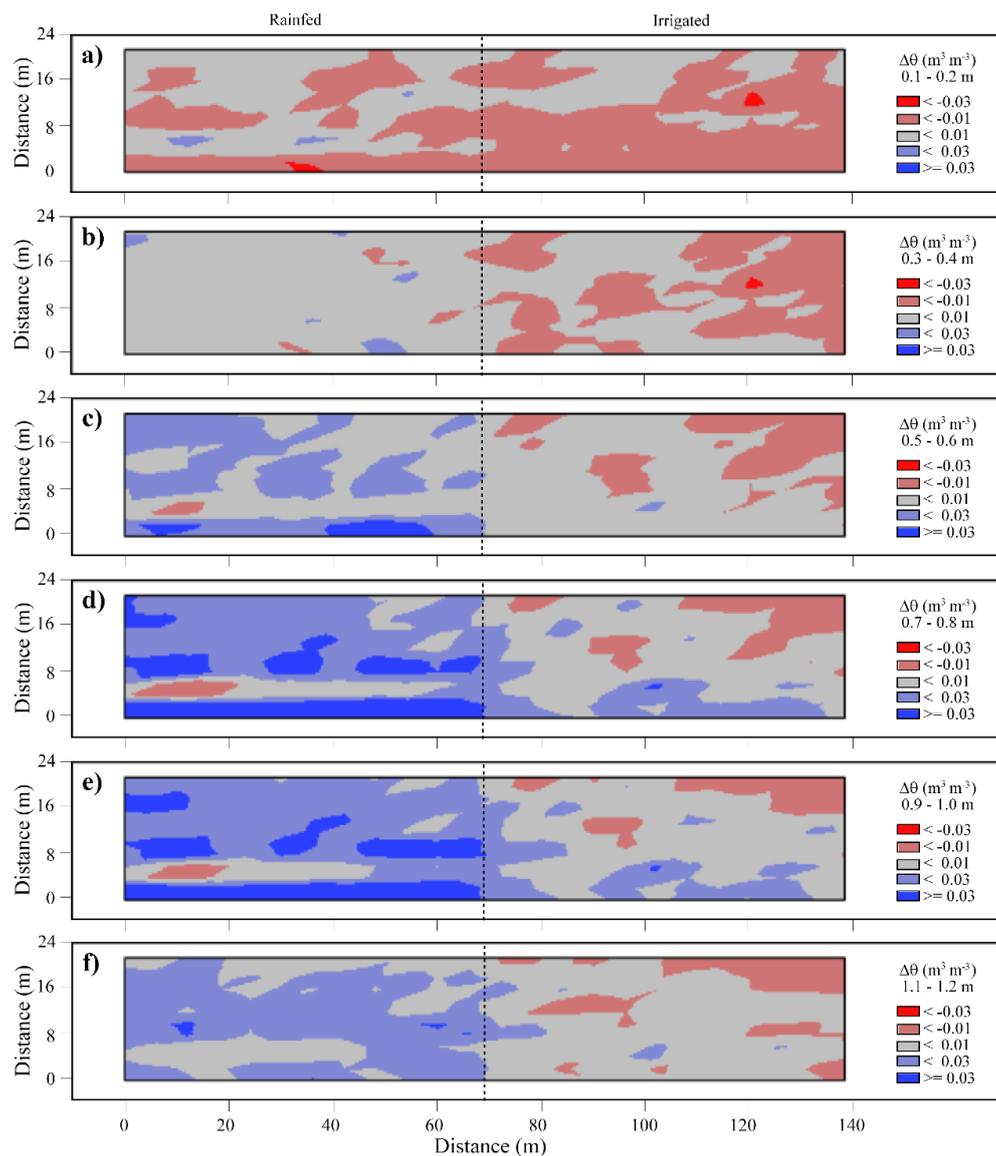
Figure 6. Contour maps of predicted change in soil volumetric water content (Δθ, $m^3\ m^{-3}$) between 1 and 9 days after a rainfall event (8-day period) at depth intervals (**a**) 0.1–0.2 m; (**b**) 0.3–0.4 m; (**c**) 0.5–0.6 m; (**d**) 0.7–0.8 m; (**e**) 0.9–1.0 m; (**f**) 1.1–1.2 m.

Figure 7 shows Δθ across the 288 plots during day 1 and day 12 (11-day period) after the rain. Compared to the first day after irrigation, θ in the rainfed plots remained unchanged. In the irrigated plots, soil continued to dry out throughout the whole profile. In particular, more water was extracted

from the deeper depths (below 0.6 m) compared with the shallow depths (Figure 7d–f). This was not unexpected because θ values at the depth of 0–0.6 m were close to the permanent wilting point of the clay soils (~0.15–0.20 m^3 m^{-3}, figures not shown) while θ in the subsoil was still high (~0.25–0.30 m^3 m^{-3}, figures not shown), so there was still available water for uptake by the chickpea genotypes.
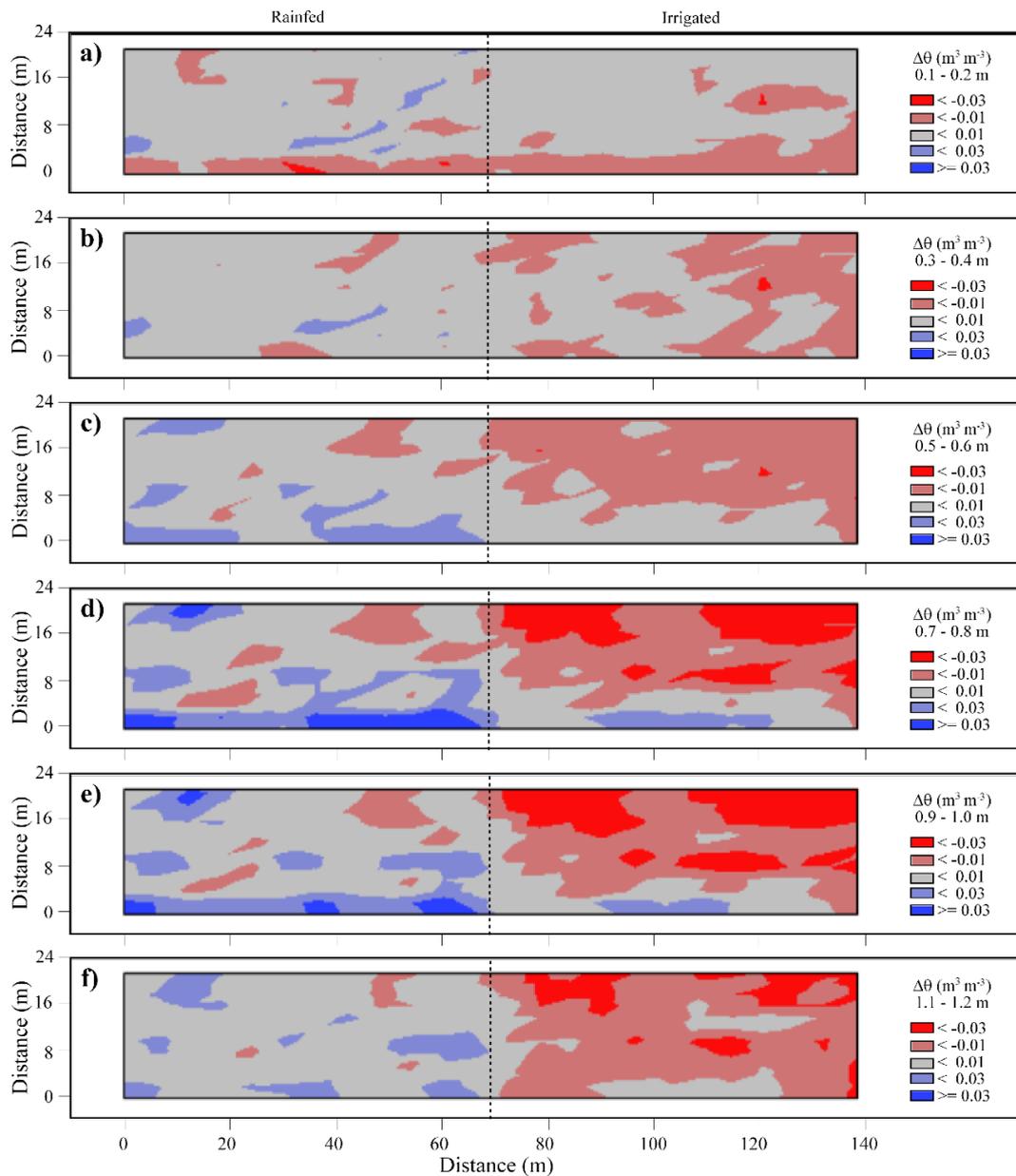
Figure 7. Contour maps of predicted change in soil volumetric water content (Δθ, m^3 m^{-3}) between 1 and 12 days after a rainfall event (11-day period) at depth intervals (**a**) 0.1–0.2 m; (**b**) 0.3–0.4 m; (**c**) 0.5–0.6 m; (**d**) 0.7–0.8 m; (**e**) 0.9–1.0 m; (**f**) 1.1–1.2 m.

Based on the results presented in Figures 5–7, it can be concluded that soil water content at the plot scale can be extremely dynamic and wetter/drier areas at one time step could either persist or change in a different direction at the next time step. This is reasonable because the crop water use is highly dynamic, depending on varieties, developmental stages and even previous soil moisture status (hysteresis effect) [46]. To validate these assumptions, sensor-based real-time monitoring of leaf turgor

pressure and stem water status coupled with plant physiological analysis [47] can be used in the future to value-add to the time-lapse 3-D images of soil water status generated using repeated EMI surveys.

3.6. Water Balance Across the Field

Averaged soil water flux (J_{depth}, mm) at different depths and within the top 1.2 m of the soils is presented in Table 1. J_{depth} values deeper than 1.2 m were not shown because θ was relatively constant during the whole experimental period. A net amount of 1.9 mm of water was added to the rainfed plots and 17.0 mm of water was removed from the irrigated plots over 11 days (day 1 to day 12) considering 12.6 mm of water was added to the soil via rainfall (Table 1). Table 1 also shows that water was first (days 3–9) removed from the shallow soil and then (days 9–12) from the deeper soil.

Table 1. Predicted averaged soil water flux (J_{depth}, mm) at different depth intervals and 0–1.2 m soil in the rainfed and irrigated plots during the study period.

Depth	Rainfed				Irrigated			
	Days 1–3	Days 3–9	Days 9–12	Days 1–12	Days 1–3	Days 3–9	Days 9–12	Days 1–12
$J_{0.0–0.1\ m}$	0.1	−0.9	0.5	−0.4	−0.2	−1.1	0.5	−0.7
$J_{0.1–0.2\ m}$	0.1	−0.9	0.5	−0.4	−0.2	−1.1	0.5	−0.7
$J_{0.2–0.3\ m}$	0.1	−0.5	0.2	−0.3	−0.2	−1.0	0.3	−0.9
$J_{0.3–0.4\ m}$	0.1	−0.1	−0.2	−0.1	−0.2	−0.8	0.0	−1.0
$J_{0.4–0.5\ m}$	0.2	0.3	−0.5	0.0	−0.2	−0.7	−0.2	−1.1
$J_{0.5–0.6\ m}$	0.2	1.0	−1.0	0.2	−0.3	−0.3	−0.7	−1.3
$J_{0.6–0.7\ m}$	0.3	1.6	−1.4	0.4	−0.3	0.1	−1.3	−1.5
$J_{0.7–0.8\ m}$	0.3	2.2	−1.9	0.6	−0.4	0.4	−1.8	−1.8
$J_{0.8–0.9\ m}$	0.2	2.2	−1.8	0.6	−0.4	0.5	−2.0	−1.9
$J_{0.9–1.0\ m}$	0.2	2.1	−1.8	0.5	−0.5	0.6	−2.1	−2.0
$J_{1.0–1.1\ m}$	0.1	2.1	−1.7	0.5	−0.6	0.7	−2.2	−2.1
$J_{1.1–1.2\ m}$	0.0	1.3	−1.0	0.2	−0.6	0.2	−1.6	−2.0
$J_{0.0–1.2\ m}$	1.7	10.4	−10.2	1.9	−4.1	−2.4	−10.5	−17.0

Therefore, the change of θ within 0–1.2 m in the rainfed plots was a function of deep percolation (1.7 mm and 10.4 mm over days 1–3 and days 3–9) and evaporation and transpiration (10.2 mm over days 9–12). This was not the case for irrigated plots. During the 11-day period, the chickpea continued to extract water from the soils with −4.1 mm, −2.4 mm, and −10.5 mm of water leaving the profiles as evaporation and transpiration.

These values were different from those reported in the loamy soils with Lucerne whereby 37 mm water leached out via deep percolation after 68 mm of irrigation water was applied [18]. The values reported here were also different from those reported in heavy clay soils with irrigated cotton, whereby an average of 42.5 mm was lost due to deep drainage with irrigation ranging from 19 to 285 mm [48]. The main reason our values are smaller is because only 12.6 mm of water was uniformly added to the soil via a rainfall event.

3.7. Variation in Chickpea Genotypic and Growth-Dependent Water Use

Table 2 shows the estimated fixed effect coefficients for different genotypes under rainfed and irrigated conditions. Only seven genotypes under the rainfed conditions were still extracting some water from the soils (indicated by negative coefficients), which is indicative of their earlier phenology induced by terminal drought. Genotype 6 in the rainfed conditions had the smallest coefficient (−0.94) and hence, the greatest water use over the 11-day period, followed by genotypes 13, 11, 32, 28, 9, and 31. This was not the case for chickpea in the irrigated half of the trial, where 26 genotypes were extracting water from the soil and the genotype 34 had the greatest water use.

Table 2. Estimated fixed effect coefficients for different chickpea genotypes under rainfed and irrigated conditions. Note: negative coefficients indicate greater water extraction. Note the change in the ranking of the genotypes with the different treatments.

Rank	Genotype (Rainfed)	Fixed Effect Coefficient	Genotype (Irrigated)	Fixed Effect Coefficient
1	6	−0.94	34	−0.85
2	13	−0.36	7	−0.76
3	11	−0.28	29	−0.65
4	32	−0.27	3	−0.57
5	28	−0.12	4	−0.54
6	9	−0.06	8	−0.49
7	31	−0.05	21	−0.45
8	25	0.06	24	−0.43
9	10	0.10	15	−0.42
10	20	0.11	26	−0.41
11	5	0.12	18	−0.40
12	22	0.20	36	−0.38
13	14	0.22	14	−0.38
14	2	0.28	25	−0.38
15	33	0.31	35	−0.35
16	35	0.33	16	−0.31
17	23	0.34	23	−0.27
18	17	0.35	5	−0.19
19	18	0.36	30	−0.18
20	29	0.36	12	−0.18
21	12	0.38	1	−0.17
22	16	0.39	27	−0.13
23	15	0.41	31	−0.12
24	30	0.43	20	−0.08
25	19	0.48	11	−0.07
26	21	0.48	2	−0.01
27	3	0.60	28	0.04
28	26	0.64	22	0.05
29	27	0.67	17	0.12
30	24	0.70	32	0.18
31	34	0.98	9	0.20
32	4	1.03	33	0.24
33	8	1.17	19	0.27
34	7	1.22	6	0.31
35	1	1.28	13	0.43
36	36	1.38	10	0.49

In addition to water use, genotypic and growth-dependent variation in root system traits were detected. Table 3 shows the mean values of water flux (J_{Depth}, mm) within each depth interval for several genotypes during the 11-day period. Genotypes 6 and 34 were used to present the genotypes that were actively extracting water during the experiment and genotypes 36 and 10 were used to present the genotypes that showed least water extraction from the soil.

Mature genotype 6 (rainfed) extracted most of the water between 0.9 m and 1.5 m (<−1.0 mm). By comparison, immature genotype 6 (irrigated) extracted water throughout the whole soil profile with the maximum water extraction between 1.1 m and 1.5 m (<−1.5 mm). This was not the case for genotype 34, which extracted water throughout the whole soil profile during both immature and mature stages. In terms of genotype 36, most of the water was extracted at the soil surface (0–0.2 m) during the mature stage and at the depth of 1.0–1.1 m during the immature stage. This was similarly the case for genotype 10, which extracted most of the water within 0–0.2 m during mature stage and within 0.7–0.8 m during the immature stage.

Table 3. Predicted averaged soil water flux (J_{depth}, mm) for several genotypes within different depth intervals in the rainfed and irrigated plots during the 11-day period.

Depth	6		34		36		10	
	Rainfed	Irrigated	Rainfed	Irrigated	Rainfed	Irrigated	Rainfed	Irrigated
$J_{0.0–0.1\ m}$	0.3	−1.0	−0.5	−0.4	−1.4	−0.3	−0.4	−1.1
$J_{0.1–0.2\ m}$	0.3	−1.0	−0.5	−0.4	−1.4	−0.3	−0.4	−1.1
$J_{0.2–0.3\ m}$	0.3	−1.0	−0.5	−0.7	−1.0	−0.6	−0.1	−1.3
$J_{0.3–0.4\ m}$	0.3	−1.0	−0.6	−1.0	−0.6	−0.8	0.1	−1.4
$J_{0.4–0.5\ m}$	0.4	−1.0	−0.6	−1.3	−0.3	−1.1	0.3	−1.6
$J_{0.5–0.6\ m}$	0.4	−1.0	−0.7	−1.8	0.3	−1.5	0.6	−1.7
$J_{0.6–0.7\ m}$	0.4	−0.9	−0.7	−2.4	0.8	−2.0	0.9	−1.8
$J_{0.7–0.8\ m}$	0.4	−0.9	−0.7	−2.9	1.4	−2.4	1.2	−2.0
$J_{0.8–0.9\ m}$	0.1	−1.0	−0.6	−3.0	1.6	−2.6	1.2	−1.9
$J_{0.9–1.0\ m}$	−0.1	−1.1	−0.4	−3.2	1.7	−2.7	1.2	−1.8
$J_{1.0–1.1\ m}$	−0.4	−1.2	−0.3	−3.3	1.9	−2.9	1.2	−1.7
$J_{1.1–1.2\ m}$	−0.8	−1.5	−0.0	−2.8	1.5	−2.5	0.8	−1.4
$J_{1.2–1.3\ m}$	−1.2	−1.7	0.2	−2.2	1.0	−2.1	0.4	−1.1
$J_{1.3–1.4\ m}$	−1.6	−2.0	0.5	−1.6	0.5	−1.7	0.0	−0.9
$J_{1.4–1.5\ m}$	−1.8	−2.1	0.7	−1.1	0.1	−1.3	−0.3	−0.7

These results suggested that the EM induction approach successfully picked up the variation in chickpea genotypic and growth-dependent water use. Because the models established between θ and EMI data are site-specific, different models need to be established to account for the variations in soil properties [6,19,21,22,43]. Given the non-invasive nature of the EMI method, the methods established in this study have the potential to be applied elsewhere at the plot scale to accelerate the traditional breeding process for estimating rooting depths across the chickpea genotypes and monitoring root activities during chickpea growth.

3.8. Caveats for Soil and Plant Scientists

Because most soil and plant scientists are not very familiar with the principles and applications of EMI instruments, we provide some caveats for them to design similar experiments for monitoring soil water dynamics at the plot scale.

(1) EMI surveys: repeated EMI surveys should be taken before and after the irrigation/rainfall events to ensure a large range of apparent electrical conductivity (EC_a) as well as θ. EMI surveys should be taken at similar ambient temperature. If a significant drift in soil temperature occurs, EC_a data need to be corrected to a standard temperature prior to further analysis using different correction formulae [18,34].

(2) Soil moisture measurements: real-time θ measurements are required to establish models between θ and EC_a data. This can be done using a number of geophysical instruments, including neutron probes, time domain reflectometry, and capacitance probes [5]. Attention should be taken to minimise the disruption of soil profiles.

(3) Model construction: it is suggested that EMI data should be inverted to calculate the depth-specific electrical conductivity (σ) for establishing a universal model between θ and σ. Examples of the inversion algorithms and model calibration approaches that have been successfully applied in the field can be found in [16,18].

4. Conclusions

It is concluded that soil water dynamics at various soil depths and movement at the plot scale can be mapped using a non-invasive EM induction instrument (i.e., EM38) and a 1-D EM inversion algorithm in heavy clay soils (Vertosols). The rate of soil drying varied with depth and was affected by the growing stages and genotypes of the chickpea. The technique is sensitive enough to characterise

differences in water use over short durations and small changes in soil moisture content, as well as different depths. The method has the potential to be used over the entire season to measure and map patterns in water use, as well as to identify genotypic and growth-dependent variation in total soil water uptake and rooting depths. Coupled with plant physiological measurements, the approach can be used to estimate root depths, to identify mechanisms of drought tolerance in the field and to screen for effective water use in crop breeding programs.

Author Contributions: For research articles with several authors, a short paragraph specifying their individual contributions must be provided. The following statements should be used "A.B.M. and H.B. conceived and designed the experiments; R.P. performed the experiments; J.H. and R.P. analyzed the data; A.B.M., H.B., R.P. and J.H. contributed reagents/materials/analysis tools; J.H., R.P., A.B.M. and H.B. wrote the paper". Authorship must be limited to those who have contributed substantially to the work reported.

Conflicts of Interest: The authors declare no conflict of interest.

References

1. Reynolds, M.; Tuberosa, R. Translational research impacting on crop productivity in drought-prone environments. *Curr. Opin. Plant. Bio.* **2008**, *11*, 171–179. [CrossRef] [PubMed]
2. Blum, A. Drought resistance, water-use efficiency, and yield potential—Are they compatible, dissonant, or mutually exclusive? *Aust. J. Agric. Res.* **2005**, *56*, 1159–1168. [CrossRef]
3. Gooley, L.; Huang, J.; Page, D.; Triantafilis, J. Digital soil mapping of available water content using proximal and remotely sensed data. *Soil Use Manag.* **2014**, *30*, 139–151. [CrossRef]
4. Jones, H.G. Monitoring plant and soil water status: Established and novel methods revisited and their relevance to studies of drought tolerance. *J. Exp. Bot.* **2006**, *58*, 119–130. [CrossRef] [PubMed]
5. Vereecken, H.; Huisman, J.A.; Pachepsky, Y.; Montzka, C.; Van Der Kruk, J.; Bogena, H.; Weihermüller, L.; Herbst, M.; Martinez, G.; Vanderborght, J. On the spatio-temporal dynamics of soil moisture at the field scale. *J. Hydrol.* **2014**, *516*, 76–96. [CrossRef]
6. Corwin, D.L.; Lesch, S.M. Application of soil electrical conductivity to precision agriculture: Theory, principles, and guidelines. *Agron J.* **2003**, *95*, 455–471. [CrossRef]
7. Doolittle, J.A.; Brevik, E.C. The use of electromagnetic induction techniques in soils studies. *Geoderma* **2014**, *223*, 33–45. [CrossRef]
8. Wong, M.T.F.; Asseng, S. Determining the causes of spatial and temporal variability of wheat yields at sub-field scale using a new method of upscaling a crop model. *Plant Soil* **2006**, *283*, 203–215. [CrossRef]
9. Aragüés, R.; Guillén, M.; Royo, A. Five-year growth and yield response of two young olive cultivars (*Olea europaea* L., cvs. Arbequina and Empeltre) to soil salinity. *Plant Soil* **2010**, *334*, 423–432. [CrossRef]
10. Li, H.Y.; Shi, Z.; Webster, R.; Triantafilis, J. Mapping the three-dimensional variation of soil salinity in a rice-paddy soil. *Geoderma* **2013**, *195*, 31–41. [CrossRef]
11. Coppola, A.; Smettem, K.; Ajeel, A.; Saeed, A.; Dragonetti, G.; Comegna, A.; Lamaddalena, A.; Vacca, A. Calibration of an electromagnetic induction sensor with time-domain reflectometry data to monitor rootzone electrical conductivity under saline water irrigation. *Eur. J. Soil Sci.* **2016**, *67*, 737–748. [CrossRef]
12. Sheets, K.R.; Hendrickx, J.M. Noninvasive soil water content measurement using electromagnetic induction. *Water Resour. Res.* **1995**, *31*, 2401–2409. [CrossRef]
13. Robinson, D.A.; Abdu, H.; Lebron, I.; Jones, S.B. Imaging of hill-slope soil moisture wetting patterns in a semi-arid oak savanna catchment using time-lapse electromagnetic induction. *J. Hydrol.* **2012**, *416*, 39–49. [CrossRef]
14. Martini, E.; Wollschläger, U.; Kögler, S.; Behrens, T.; Dietrich, P.; Reinstorf, F.; Schmidt, K.; Weiler, M.; Werban, U.; Zacharias, S. Spatial and temporal dynamics of hillslope-scale soil moisture patterns: Characteristic states and transition mechanisms. *Vadose Zone J.* **2015**, *14*. [CrossRef]

15. Von Hebel, C.; Rudolph, S.; Mester, A.; Huisman, J.A.; Kumbhar, P.; Vereecken, H.; van der Kruk, J. Three-dimensional imaging of subsurface structural patterns using quantitative large-scale multiconfiguration electromagnetic induction data. *Water Resour. Res.* **2014**, *50*, 2732–2748. [CrossRef]

16. Huang, J.; Scudiero, E.; Clary, W.; Corwin, D.L.; Triantafilis, J. Time-lapse monitoring of soil water content using electromagnetic conductivity imaging. *Soil Use Manag.* **2017**, *33*, 191–204. [CrossRef]

17. Hedley, C.B.; Roudier, P.; Yule, I.J.; Ekanayake, J.; Bradbury, S. Soil water status and water table depth modelling using electromagnetic surveys for precision irrigation scheduling. *Geoderma* **2013**, *199*, 22–29. [CrossRef]

18. Huang, J.; McBratney, A.B.; Minasny, B.; Triantafilis, J. Monitoring and modelling soil water dynamics using electromagnetic conductivity imaging and the ensemble Kalman filter. *Geoderma* **2017**, *285*, 76–93. [CrossRef]

19. Farahani, H.J.; Buchleiter, G.W.; Brodahl, M.K. Characterization of apparent soil electrical conductivity variability in irrigated sandy and non-saline fields in Colorado. *Am. Soc. Agric. Eng.* **2005**, *48*, 155–168. [CrossRef]

20. Shanahan, P.W.; Binley, A.; Whalley, W.R.; Watts, C.W. The use of electromagnetic induction to monitor changes in soil moisture profiles beneath different wheat genotypes. *Soil Sci. Soc. Am. J.* **2015**, *79*, 459–466. [CrossRef]

21. Altdorff, D.; von Hebel, C.; Borchard, N.; van der Kruk, J.; Bogena, H.R.; Vereecken, H.; Huisman, J.A. Potential of catchment-wide soil water content prediction using electromagnetic induction in a forest ecosystem. *Environ. Earth Sci.* **2017**, *76*, 111. [CrossRef]

22. Martini, E.; Werban, U.; Zacharias, S.; Pohle, M.; Dietrich, P.; Wollschläger, U. Repeated electromagnetic induction measurements for mapping soil moisture at the field scale: Validation with data from a wireless soil moisture monitoring network. *Hydrol. Earth Syst. Sci.* **2017**, *21*, 495–513. [CrossRef]

23. Stanley, J.N.; Lamb, D.W.; Falzon, G.; Schneider, D.A. Apparent electrical conductivity (EC$_a$) as a surrogate for neutron probe counts to measure soil moisture content in heavy clay soils (Vertosols). *Soil Res.* **2014**, *52*, 373–378. [CrossRef]

24. Weatherzone. Available online: http://www.weatherzone.com.au/climate/station.jsp?lt=site&lc=53030 (accessed on 27 January 2018).

25. Isbell, R. *The Australian Soil Classification*; CSIRO publishing: Melbourne, Australia, 2002.

26. McNeill, J.D. *Geonics EM38 Ground Conductivity Meter: EM38 Operating Manual*; Geonics Ltd.: Mississauga, ON, Canada, 1990.

27. Borchers, B.; Uram, T.; Hendrickx, J.M. Tikhonov regularization of electrical conductivity depth profiles in field soils. *Soil Sci. Soc. Am. J.* **1997**, *61*, 1004–1009. [CrossRef]

28. Hendrickx, J.M.H.; Borchers, B.; Corwin, D.L.; Lesch, S.M.; Hilgendorf, A.C.; Schlue, J. Inversion of soil conductivity profiles from electromagnetic induction measurements. *Soil Sci. Soc. Am. J.* **2002**, *66*, 673–685. [CrossRef]

29. Huang, J.; Taghizadeh-Mehrjardi, R.; Minasny, B.; Triantafilis, J. Modeling soil salinity along a hillslope in Iran by inversion of EM38 data. *Soil Sci. Soc. Am. J.* **2015**, *79*, 1142–1153. [CrossRef]

30. Reedy, R.C.; Scanlon, B.R. Soil water content monitoring using electromagnetic induction. *J. Geotech. Geoenviron.* **2003**, *129*, 1028–1039. [CrossRef]

31. Brevik, E.C.; Fenton, T.E.; Horton, R. Effect f daily soil temperature fluctuations on soil electrical conductivity as measured with the Geonics® EM-38. *Precis. Agric.* **2004**, *5*, 143–150. [CrossRef]

32. Allred, B.J.; Ehsani, M.R.; Saraswat, D. The impact of temperature and shallow hydrologic conditions on the magnitude and spatial pattern consistency of electromagnetic induction measured soil electrical conductivity. *Trans. Am. Soc. Agric. Eng.* **2005**, *48*, 2123–2135. [CrossRef]

33. Tromp-van Meerveld, H.J.; McDonnell, J.J. Assessment of multi-frequency electromagnetic induction for determining soil moisture patterns at the hillslope scale. *J. Hydrol.* **2009**, *368*, 56–67. [CrossRef]

34. Ma, R.; McBratney, A.; Whelan, B.; Minasny, B.; Short, M. Comparing temperature correction models for soil electrical conductivity measurement. *Precis. Agric.* **2011**, *12*, 55–66. [CrossRef]

35. Robinet, J.; von Hebel, C.; Govers, G.; van der Kruk, J.; Minella, J.P.G.; Schlesner, A.; Ameijeiras-Mariño, Y.; Vanderborght, J. Spatial variability of soil water content and soil electrical conductivity across scales derived from Electromagnetic Induction and Time Domain Reflectometry. *Geoderma* **2018**, *314*, 160–174. [CrossRef]

36. Huang, J.; Minasny, B.; Whelan, B.M.; McBratney, A.B.; Triantafilis, J. Temperature-dependent hysteresis effects on DUALEM instruments. *Comput. Electron. Agric.* **2017**, *132*, 76–85. [CrossRef]

37. Sudduth, K.A.; Drummond, S.T.; Kitchen, N.R. Accuracy issues in electromagnetic induction sensing of soil electrical conductivity for precision agriculture. *Comput. Electron. Agric.* **2001**, *31*, 239–264. [CrossRef]

38. Monteiro Santos, F.A. 1-D laterally constrained inversion of EM34 profiling data. *J. Appl. Geophys.* **2004**, *56*, 123–134. [CrossRef]

39. Lark, R.M.; Cullis, B.R.; Welham, S.J. On spatial prediction of soil properties in the presence of a spatial trend: The empirical best linear unbiased predictor (E-BLUP) with REML. *Eur. J. Soil Sci.* **2006**, *57*, 787–799. [CrossRef]

40. Ribeiro, P.J., Jr.; Diggle, P.J. geoR: A package for geostatistical analysis. *R News* **2001**, *1*, 14–18.

41. Lin, L.I.K. A concordance correlation coefficient to evaluate reproducibility. *Biometrics* **1989**, *45*, 255–268. [CrossRef] [PubMed]

42. Arslan, A.; Razzouk, A.K.; Al-Ain, F. The performance and radiation exposure of some neutron probes in measuring the water content of the topsoil layer. *Soil Res.* **1997**, *35*, 1397–1407. [CrossRef]

43. Corwin, D.L.; Lesch, S.M.; Farahani, H. Theoretical insight on the measurement of soil electrical conductivity. In *Handbook of Agricultural Geophysics*; Allred, B.J., Daniels, J.J., Ehsani, M.R., Eds.; CRC Press: Boca Raton, FL, USA, 2008; pp. 59–83.

44. Martínez, G.; Vanderlinden, K.; Giráldez, J.V.; Espejo, A.J.; Muriel, J.L. Field-scale soil moisture pattern mapping using electromagnetic induction. *Vadose Zone J.* **2010**, *9*, 871–881. [CrossRef]

45. Martínez, G.; Huang, J.; Vanderlinden, K.; Giráldez, J.V.; Triantafilis, J. Potential to predict depth-specific soil water content beneath an olive tree using electromagnetic conductivity imaging. *Soil Use Manag.* **2018**, in press.

46. Siqueira, M.; Katul, G.; Porporato, A. Onset of water stress, hysteresis in plant conductance, and hydraulic lift: Scaling soil water dynamics from millimeters to meters. *Water Resour. Res.* **2008**, *44*. [CrossRef]

47. Bramley, H.; Bitter, R.; Zimmermann, G.; Zimmermann, U. Simultaneous recording of diurnal changes in leaf turgor pressure and stem water status of bread wheat reveal variation in hydraulic mechanisms in response to drought. *Funct. Plant Boil.* **2015**, *42*, 1001–1009. [CrossRef]

48. Smith, R.J.; Raine, S.R.; Minkevich, J. Irrigation application efficiency and deep drainage potential under surface irrigated cotton. *Agric. Water Manag.* **2005**, *71*, 117–130. [CrossRef]